

CHEMICAL SIGNATURES OF THE FIRST SUPERNOVAE IN THE SCULPTOR DWARF SPHEROIDAL GALAXY*

JOSHUA D. SIMON¹, HEATHER R. JACOBSON², ANNA FREBEL², IAN B. THOMPSON¹, JOSHUA J. ADAMS³, AND STEPHEN A. SHECTMAN¹

Accepted for publication in ApJ

ABSTRACT

We present a homogeneous chemical abundance analysis of five of the most metal-poor stars in the Sculptor dwarf spheroidal galaxy. We analyze new and archival high resolution spectroscopy from Magellan/MIKE and VLT/UVES and determine stellar parameters and abundances in a consistent way for each star. Two of the stars in our sample, at $[\text{Fe}/\text{H}] = -3.5$ and $[\text{Fe}/\text{H}] = -3.8$, are new discoveries from our Ca K survey of Sculptor, while the other three were known in the literature. We confirm that Scl 07-50 is the lowest metallicity star identified in an external galaxy, at $[\text{Fe}/\text{H}] = -4.1$. The two most metal-poor stars both have very unusual abundance patterns, with striking deficiencies of the α elements, while the other three stars resemble typical extremely metal-poor Milky Way halo stars. We show that the star-to-star scatter for several elements in Sculptor is larger than that for halo stars in the same metallicity range. This scatter and the uncommon abundance patterns of the lowest metallicity stars indicate that the oldest surviving Sculptor stars were enriched by a small number of earlier supernovae, perhaps weighted toward high-mass progenitors from the first generation of stars the galaxy formed.

Keywords: galaxies: dwarf; galaxies: individual (Sculptor dSph); galaxies: stellar content; stars: abundances

1. INTRODUCTION

Metal-poor stars represent the local equivalent of the high-redshift universe and supply us with a uniquely detailed view of the conditions in early galaxies. The lowest metallicity stars in dwarf galaxies are particularly enticing targets for chemical abundance studies because dwarfs have simpler merging and evolutionary histories than more massive systems like the Milky Way.

The first extremely metal-poor (EMP) stars with $[\text{Fe}/\text{H}] \leq -3.0$ in nearby dwarf galaxies were discovered by Kirby et al. (2008). Over the past five years, a sizable sample of such stars has been identified and analyzed, in both the ultra-faint dwarfs and the brighter classical dwarf spheroidals (Aoki et al. 2009; Cohen & Huang 2009, 2010; Frebel, Kirby, & Simon 2010a; Frebel et al. 2010b; Simon et al. 2010; Norris et al. 2010a,b; Tafelmeyer et al. 2010; Kirby & Cohen 2012; Gilmore et al. 2013; Starkenburg et al. 2013; Frebel, Simon, & Kirby 2014; Ishigaki et al. 2014). The initial results of these studies were that EMP stars in dwarf galaxies appear remarkably similar to EMP stars in the Milky Way, suggesting that early chemical evolution is largely independent of galactic environment (e.g., Frebel et al. 2010a,b; Simon et al. 2010). Now that a statistically significant number of EMP stars beyond the Milky Way are available, we can begin to examine this conclusion more care-

fully, and search for outliers from the typical abundance pattern rather than simply characterizing broad trends within the population.

In this paper we present a homogeneous detailed chemical abundance analysis of five of the most metal-poor stars in the Sculptor dwarf spheroidal (dSph), with $[\text{Fe}/\text{H}] \leq -3.2$. Three of these stars have been studied previously by Tafelmeyer et al. (2010, hereafter T10) and Frebel et al. (2010a), but we re-analyze those data with a common set of methods and assumptions. We also add two new EMP stars identified on the basis of their weak Ca K absorption in our Magellan search for the most metal-poor stars in the Milky Way's southern dSphs, and determine their chemical abundance patterns with high resolution spectroscopy for the first time. Additional descriptions of the survey and the resulting sample of EMP stars will be provided in future papers. In Section 2 we describe the data used in this study and the reduction methods. We present the chemical abundance measurements in Section 3, and we discuss the abundance patterns and their implications for the early history of Sculptor in Section 4. We summarize the paper in Section 5.

2. OBSERVATIONS AND DATA REDUCTION

We selected Scl 6.6_402 and Scl 11.1_4296 as candidate Sculptor members from the photometry catalog of Coleman, Da Costa, & Bland-Hawthorn (2005). We obtained $R \approx 700$ spectra centered on the Ca K line of ~ 2000 such stars with the f/2 camera of the IMACS spectrograph (Dressler et al. 2011) from 2009 – 2011. These were two of the stars with the smallest Ca K equivalent widths in the sample, marking them as likely EMP stars. We obtained medium resolution Magellan/MagE (Marshall et al. 2008) spectra of them in 2010 December, confirming their extremely low metallicity. We then

* This paper includes data gathered with the 6.5 meter Magellan Telescopes located at Las Campanas Observatory, Chile.

¹ Observatories of the Carnegie Institution of Washington, 813 Santa Barbara St., Pasadena, CA 91101; jsimon, ian.jjadams, shec@obs.carnegiescience.edu

² Kavli Institute for Astrophysics and Space Research and Department of Physics, Massachusetts Institute of Technology, 77 Massachusetts Avenue, Cambridge, MA 02139; hjr.afrebel@mit.edu

³ ASML US, 77 Danbury Rd., Wilton, CT 06897

observed the two stars with Magellan/MIKE (Bernstein et al. 2003) at $R \approx 25000$ over a wavelength range of 3460 – 9410 Å on ten nights between 2013 October and 2014 June, accumulating a total of 20 hr of integration time on Scl 6_6_402 and 9.7 hr on Scl 11_1_4296. The MIKE spectra were reduced with the Carnegie Python routines originally described by Kelson (2003).

Two other EMP stars in Sculptor, Scl 07-49 and Scl 07-50, were identified by T10 in the data set of the Dwarf Abundances and Radial velocities Team (Tolstoy et al. 2004; Helmi et al. 2006) using the Ca triplet metallicity calibration from Starkenburg et al. (2010). T10 obtained $R \approx 40000$ spectra of these stars with VLT/UVES (Dekker et al. 2000) and measured their chemical abundances. The spectrum of Scl 07-50 was obtained with both the red and blue arms of UVES, covering 3700 – 10200 Å, while Scl 07-49 was observed only with the red arm (4700–10200 Å). To ensure that the full sample can be placed on a common abundance scale we downloaded the reduced spectra from the ESO archive and analyzed them with the same method we followed for the other stars (see § 3). The data available online are individual exposures processed by version 5.1.5 of the UVES pipeline, which handles standard reduction procedures and merges the echelle orders. We then normalized the spectra and coadded the frames for each star. For further details on the observations, see T10.

S1020549 was identified by Kirby et al. (2009) as an EMP star at $[\text{Fe}/\text{H}] = -3.8$ (at the time the most metal-poor star in an external galaxy) based on medium resolution Keck/DEIMOS spectroscopy. Frebel et al. (2010a) confirmed that result and analyzed its chemical abundance pattern with an $R \approx 33000$ Magellan/MIKE spectrum covering the same wavelength range as our new MIKE data. We use that spectrum again here, but as for Scl 07-49 and Scl 07-50 we re-measure the equivalent widths and re-determine the stellar parameters and chemical abundances.

3. DETERMINATION OF STELLAR PARAMETERS AND CHEMICAL ABUNDANCES

3.1. Measurement Procedures

We measured the equivalent widths (EWs) of metal lines in the spectra by fitting a Gaussian to each absorption line and integrating the area under the Gaussian. The lines were selected from the line list constructed by Roederer et al. (2008). Where available, we have adopted collisional damping constants from Barklem et al. (2000); for other lines we used the Unsold (1955) approximation. We set the continuum of each spectrum by fitting a low-order cubic spline to each spectral order. Because the spectra of these faint stars have low S/N, the placement of the continuum can be challenging, especially at blue wavelengths.

Our derivation of the stellar parameters closely follows that of Frebel et al. (2014) and Frebel et al. (2013): using the analysis code of Casey (2014), we employ α -enhanced one-dimensional plane-parallel ATLAS9 model atmospheres from Castelli & Kurucz (2004) and the MOOG stellar analysis code (Sneden 1973) updated to include a treatment of Rayleigh scattering (Sobeck et al. 2011). We assume local thermodynamic equilibrium throughout this paper, except where otherwise noted.

Starting from the EW measurements, we computed effective temperatures and surface gravities in the usual manner by enforcing ionization and excitation balance of iron line abundances. The microturbulent velocity was derived iteratively by minimizing the trend of Fe I abundance with reduced equivalent width. We then corrected these spectroscopic parameters according to the prescription of Frebel et al. (2013) to place the measurements on the same scale as studies that calculate stellar parameters from photometry alone. As a check of this process, we also calculated photometric temperatures using $V - K_s$ colors determined from the optical photometry of Coleman et al. (2005) and the near-infrared photometry of Menzies et al. (2011) and the Alonso, Arribas, & Martínez-Roger (1999) color-temperature relation. The photometric temperatures of Scl 11_1_4296, Scl 6_6_402, and S1020549 are within 100 K of our adopted values. For Scl 07-50 and Scl 07-49 the colors suggest temperatures that are 200 – 300 K warmer. T10 find a temperature for Scl 07-49 that is in agreement with ours rather than the photometric value, but they prefer a higher temperature for Scl 07-50.⁵ Because the quality of the spectrum for Scl 07-50 is relatively high and so many iron lines can be included in our analysis, we consider the spectroscopically derived temperature more likely to be accurate. We also note that Frebel et al. (2013) showed that the microturbulent velocity determined with this method is in good agreement with values obtained by other authors in the literature.

We list the derived stellar parameters for each star in Table 1, the EWs in Table 2, and the abundances in Table 3. All abundance ratios have been calculated using the Asplund et al. (2009) solar abundance scale. We estimate the systematic uncertainties on the derived abundances by adjusting the atmospheric parameters by their uncertainties (see Table 1) and re-determining the abundance ratios. The uncertainties on each element as a result of changing T_{eff} , $\log g$ and the microturbulent velocity for each star are listed in Table 4. The statistical uncertainties for elements with multiple lines are defined to be equal to the dispersion in the abundance ratio about the mean value divided by the square root of the number of lines. In cases where this dispersion is unrealistically small, we impose a minimum value of 0.10 dex. Following Frebel et al. (2010b), who analyzed similar stars with spectra of similar quality, we adopt a minimum abundance uncertainty of 0.2 dex for elements where abundances are measured from a single line. The total uncertainty for each element is the sum in quadrature of the above terms.

3.2. Comparison to Literature Measurements

Since three of the stars in our sample have been analyzed in the literature using the same spectra we employ, we compare the abundance results to check for differences resulting from assumptions or methodology. Our results for S1020549 agree with those of Frebel et al. (2010a) within 1 σ (where σ here refers to the quadrature sum

⁵ The K_s magnitudes for these two stars are ~ 0.16 mag fainter in Menzies et al. (2011) than in the VISTA commissioning data reported by T10, which could account for a temperature shift of ~ 200 K, but neither paper contains enough information about the photometric calibration to determine which one is correct.

Table 1
Coordinates and Stellar Parameters

Star	R.A. (J2000)	Decl. (J2000)	V	$V - I$	$V - K_s$	T_{eff} [K]	$\log g$ [dex]	v_{micr} [km s $^{-1}$]	[Fe/H] [dex]	S/N ^a
ScI 11_1_4296	00:59:38.75	-33:46:14.6	19.16	1.12	2.31	4770 \pm 150	1.45 \pm 0.3	1.90 \pm 0.3	-3.77	84
ScI 6_6_402	01:00:00.39	-33:29:15.2	19.13	1.07	2.19	4945 \pm 150	2.00 \pm 0.3	1.80 \pm 0.3	-3.53	76
ScI 07-50	01:00:01.12	-33:59:21.4	18.67	1.16	2.37	4558 \pm 150	1.05 \pm 0.3	2.35 \pm 0.3	-4.05	190
ScI 07-49	01:00:05.00	-34:01:16.6	18.38	1.19	2.46	4495 \pm 150	0.80 \pm 0.3	2.65 \pm 0.3	-3.31	204
S1020549	01:00:47.83	-33:41:03.2	18.34	1.20	2.51	4702 \pm 150	1.25 \pm 0.3	2.30 \pm 0.3	-3.68	171

Note. — Coordinates and optical magnitudes are taken from Coleman et al. (2005). K_s magnitudes are from Menzies et al. (2011).

^a The signal-to-noise ratio is given per Å, measured at a wavelength of 5350 Å.

of the uncertainties in our measurements and those determined by Frebel et al.) for all elements except Mg, where our value of [Mg/Fe] is higher by 0.47 dex (1.5 σ).

Our agreement with T10 is reasonable, although slightly less good, with 14 of 26 measurements (covering both ScI 07-50 and ScI 07-49) matching to 1 σ . The Fe I abundances we measure agree with those determined by T10 ($\Delta[\text{Fe}/\text{H}] = -0.09 \pm 0.21$ dex for ScI 07-50 and $\Delta[\text{Fe}/\text{H}] = +0.17 \pm 0.20$ dex for ScI 07-49), but with our stellar parameters there is no significant difference between Fe I and Fe II. Even though these metallicity differences are not statistically significant, they factor into more significant differences of abundance ratios with respect to iron for some other elements (see below). We therefore conduct a detailed comparison of our [Fe/H] measurements with those of T10 by examining the EWs of lines in common. Our EWs are systematically lower than those of T10, by an average of ~ 3 mÅ for all lines and ~ 5 mÅ for Fe lines. This EW offset would lead to a decrease of $\sim 0.1 - 0.2$ dex in [Fe/H] if the corresponding changes in stellar parameters were ignored. We note that our abundance determination uses many more lines than T10 did: 92 and 54 Fe I lines for ScI 07-49 and ScI 07-50, respectively, compared to 22 and 25. We consider the most likely explanation for the modest changes in [Fe/H] we derive to be a combination of continuum placement, the lines used, and the different methods for determining stellar parameters.

Of the differences in other elements for ScI 07-50 and ScI 07-49, most are of modest significance ($\lesssim 1.7 \sigma$). The exceptions are [Mg/Fe], where our measurements are higher by 1.7 σ and 3.0 σ , respectively, [Sc/Fe], where our measurements are lower by 1.7 – 2.6 σ , and [Ca/Fe] (for ScI 07-50 only), where our value is 1.7 σ higher. Addressing Mg first, the primary difference for ScI 07-50 is our EW measurements, which are ~ 8 mÅ larger. This EW offset increases $\log \epsilon(\text{Mg})$ by 0.18 dex, which when combined with our lower [Fe/H] results in [Mg/Fe] increasing by 0.27 dex. Our $\log gf$ values for the Mg b lines are smaller than those used by T10, which accounts for the remainder of the increase in [Mg/Fe]. For ScI 07-49 the offset in EWs relative to T10 is somewhat smaller, but in the same sense. The difference in stellar parameters is responsible for changing the Mg abundance by 0.16 dex. However, our calculations of $\log \epsilon(\text{Mg})$ using T10’s EWs and stellar parameters yield $\log \epsilon(\text{Mg}) = 4.62$, while their reported value is 4.32, suggesting the possibility of unexpectedly large differences between their model atmosphere calculations and ours.

For Sc, the comparison is complicated by varying treatments of hyperfine splitting and EW vs. spectral synthesis measurements, but there are significant differences resulting from stellar parameters (0.26 dex for ScI 07-50 and 0.13 dex for ScI 07-49). The difference in iron abundances makes the disagreement in [Sc/Fe] smaller than the disagreement in $\log \epsilon(\text{Sc})$ for ScI 07-50, but the reverse is true for ScI 07-49. After factoring in changes in stellar parameters and [Fe/H], our Sc abundances are still lower than those of T10 by 0.2 – 0.3 dex, which may result from differences in the measured strength of the Sc lines and/or differences in stellar atmospheres and analysis methods. Finally, for Ca, our larger EW results in an abundance that is higher by 0.21 dex. This is partially counteracted by the difference in stellar parameters, which lower $\log \epsilon(\text{Ca})$, but as with Mg the combination of a higher Ca abundance and a lower Fe abundance results in a substantial shift in [Ca/Fe]. Also similar to Mg, we find that even if we use T10’s EWs and stellar parameters we get a value of $\log \epsilon(\text{Ca})$ that differs from theirs by 0.18 dex.

4. DISCUSSION

4.1. Iron Peak Elements

The newly discovered EMP stars ScI 6_6_402 and ScI 11_1_4296 have [Fe/H] = -3.53 and [Fe/H] = -3.77, respectively, ranking both among the ten lowest metallicity stars known beyond the Milky Way.

For the two stars previously studied by T10, as mentioned in § 3.2, we find Fe I abundances that are in agreement within the uncertainties. Our measurements are [Fe/H] = -3.31 for ScI 07-49 and [Fe/H] = -4.05 for ScI 07-50. We note that while ScI 07-50 is only slightly more metal-poor in our analysis, it now formally qualifies as the first ultra metal-poor star identified in an external galaxy according to the nomenclature proposed by Beers & Christlieb (2005). For S1020549 we obtain [Fe/H] = -3.68, in agreement with our earlier determination within the uncertainties (Frebel et al. 2010a).

For the other iron-peak elements Sc, Cr, Mn, Co, Ni, and Zn the abundance patterns of the ScI stars are broadly consistent with those seen in the Milky Way halo at similar metallicities (see Figure 1). The Co abundances tend to be higher than those of most halo stars, while the Mn abundances for three of the Sculptor stars are near the lower bound of [Mn/Fe] observed in EMP halo stars. ScI 11_1_4296 and especially ScI 07-49 have Mn abundances above the halo average, but the value for the latter star is determined only from two weak lines be-

Table 4
Abundance Uncertainties (abridged)

Star	[X/Fe]	$\sigma_{\text{obs}}^{\text{a}}$	ΔT_{eff} +150 K	$\Delta \log g$ +0.3 dex	Δv_{t} +0.3 km s ⁻¹	Total ^b
Scl 11_1_4296	CH	0.20	+0.26	-0.09	-0.01	0.34
	Na I	0.07	-0.04	+0.03	+0.08	0.12
	Mg I	0.06	-0.16	+0.00	+0.03	0.17
	Al I	0.20	-0.04	+0.02	+0.08	0.22
	Si I	0.20	-0.04	+0.00	-0.01	0.20
	Ca I	0.20	-0.01	-0.02	-0.06	0.21
	Sc II	0.20	-0.08	+0.12	-0.02	0.25
	Ti I
	Ti II	0.04	-0.12	+0.13	+0.06	0.19
	Cr I	0.11	-0.01	+0.02	+0.06	0.13
	Mn I	0.07	+0.01	+0.02	+0.06	0.09
	Fe I ^c	0.04	+0.19	-0.06	-0.14	0.25
	Fe II ^c	0.07	+0.03	+0.09	-0.03	0.12
	Co I
	Ni I
	Zn I
	Sr II	...	-0.09	+0.11	+0.09	0.17
	Ba II	...	-0.01	+0.16	+0.19	0.25
Eu II	
Scl 6_6_402	CH	0.20	+0.15	-0.10	+0.13	0.30
	Na I	0.11	-0.03	+0.02	+0.04	0.12
	Mg I	0.09	+0.01	-0.08	+0.00	0.12
	Al I	0.20	-0.06	+0.02	+0.10	0.23
	Si I	...	-0.06	+0.04	+0.11	0.13
	Ca I	0.20	-0.03	-0.03	+0.01	0.20
	Sc II	0.08	-0.10	+0.13	+0.08	0.20
	Ti I
	Ti II	0.12	-0.12	+0.14	+0.09	0.24
	Cr I
	Mn I	0.13	-0.01	+0.02	+0.09	0.16
	Fe I ^c	0.04	+0.21	-0.04	-0.13	0.25
	Fe II ^c	0.05	+0.03	+0.10	-0.04	0.12
	Co I	0.20	+0.01	+0.02	-0.01	0.20
	Ni I	0.07	-0.03	+0.02	+0.03	0.08
	Zn I
	Sr II	0.20	-0.09	+0.20	+0.03	0.30
	Ba II	0.20	-0.08	+0.10	+0.06	0.24
Eu II	...	+0.16	+0.36	+0.34	0.52	
Scl 07-50	CH	0.20	+0.22	-0.11	+0.08	0.34
	Na I	0.07	-0.01	+0.01	+0.02	0.08
	Mg I	0.05	-0.08	-0.07	-0.07	0.13
	Al I	0.07	-0.03	-0.03	+0.00	0.08
	Si I	0.20	-0.09	-0.08	-0.10	0.25
	Ca I	0.20	-0.06	-0.08	-0.12	0.26
	Sc II	0.06	-0.07	+0.12	+0.04	0.16
	Ti I
	Ti II	0.03	-0.10	+0.12	+0.05	0.17
	Cr I	0.06	+0.04	+0.01	+0.06	0.07
	Mn I	0.07	+0.09	+0.02	+0.07	0.11
	Fe I ^c	0.02	+0.17	-0.05	-0.08	0.20
	Fe II ^c	0.11	+0.00	+0.09	-0.02	0.14
	Co I	0.06	+0.06	+0.01	+0.05	0.08
	Ni I	0.06	+0.03	-0.01	+0.00	0.07
	Zn I
	Sr II	0.07	-0.05	+0.11	+0.04	0.16
	Ba II	0.20	-0.03	+0.11	+0.07	0.25
Eu II	...	-0.06	+0.11	+0.08	0.38	

Note. — Only a portion of the table is shown in the arXiv version of the paper. Please contact the first author or refer to the published version for the full table.

^a Dispersion of the abundance ratio about the mean for the species, divided by the square root of the number of lines, taken from Table 3. A minimum dispersion (before accounting for the number of lines) of 0.1 dex is imposed. Species for which the abundance is determined from a single line are given a dispersion of 0.2 dex.

^b Sum in quadrature of σ_{obs} , ΔT_{eff} , $\Delta \log g$, and Δv_{t} .

^c [X/H] ratios are listed instead of [X/Fe] for Fe I and Fe II.

cause of the lack of blue spectral coverage. Our spectra of the other four stars extend to shorter wavelengths, allowing us to use the much stronger Mn I $\lambda 4030$ Å triplet resonance lines. The corrections for non-LTE (NLTE) behavior in these lines are significant (e.g., Cayrel et al. 2004; Lai et al. 2008; Bergemann & Gehren 2008), and we adopt an NLTE correction of +0.30 dex to abundances determined from the Mn triplet. The only other potential outlier among the iron-peak species is the low Ni abundance of Scl 07-50, which is comparable to the lowest [Ni/Fe] values seen at [Fe/H] < -3.5 in the halo.

4.2. α -Elements

The abundance patterns of the α -elements in the Sculptor EMP stars closely follow the well-established behavior of EMP Milky Way halo stars (e.g., McWilliam et al. 1995; Cayrel et al. 2004; Cohen et al. 2013; Yong et al. 2013; Roederer et al. 2014) down to [Fe/H] = -3.7. Above this metallicity Mg, Ca, Si, and Ti lie almost perfectly along the median of the Milky Way halo distribution (see Figure 1). However, the two lowest metallicity stars show some striking differences, both from each other and from their more metal-rich counterparts: Scl 11.1.4296 has uniformly low α abundances (except Ti), while Scl 07-50 has low Ca and Si but an almost normal [Mg/Fe] ratio.

For the stars below [Fe/H] = -3.7, our Ca abundances are determined from the only Ca I line detected, the 4226.73 Å resonance line. This line is known to produce lower Ca abundances than other Ca I lines for EMP stars, at least in part because of NLTE effects (e.g., Spite et al. 2012), leading T10 to dismiss the significance of the even lower [Ca/Fe] ratio they derived for Scl 07-50. However, NLTE models do not agree well on the correction for the 4226.73 Å line for stars with similar atmospheric parameters to Scl 07-50 and Scl 11.1.4296, with recent predictions ranging from -0.02 dex (Starkenburg et al. 2010) to +0.21 dex (Mashonkina, Korn, & Przybilla 2007, L. Mashonkina 2014, personal communication). We therefore attempted several additional tests to verify the low Ca abundances. First, we compared the Ca lines of both stars with those of the ultra metal-poor giant CD-38°245 (Bessell & Norris 1984), which is comparable in temperature to Scl 11.1.4296 and ~ 200 K warmer than Scl 07-50 (see Figure 2). Scl 11.1.4296 has weaker Ca I $\lambda 4226.73$ Å and near-infrared Ca II triplet lines than CD-38°245, confirming its low Ca abundance. Scl 07-50 has similar Ca K and Ca I $\lambda 4226.73$ Å EWs to CD-38°245, consistent with a lower Ca abundance given the temperature difference.⁶ Second, we compared to stars with similar parameters (after adjusting their spectroscopic temperatures according to the Frebel et al. 2013 formula) from Roederer et al. (2014). These stars were selected to have $4400 \text{ K} < T_{\text{eff}} < 4900 \text{ K}$, $-0.2 < \log g < 1.8$, [Fe/H] < -3, and a detection of the Ca I resonance line, resulting in a sample of 13 stars. For this sample, Ca abundances from Ca I 4226.73 Å are 0.09 dex lower than the mean abundance from all other Ca I lines.⁷ This offset is in excellent agreement with

the most recent NLTE corrections for Ca determined by Spite et al. (2012), which give 0.08 dex for $T_{\text{eff}} = 4750 \text{ K}$, $\log g = 1$, [Ca/H] = -3.2. Finally, we stacked the four strongest Ca I non-resonance lines and determined upper limits of [Ca/Fe] < -0.06 dex and [Ca/Fe] < -0.12 dex for Scl 07-50 and Scl 11.1.4296, respectively, by comparing to synthesized spectra. We therefore conclude that even after factoring in the uncertain NLTE effects, Scl 07-50 and Scl 11.1.4296 indeed have low Ca abundances.

Using the large halo samples of Cohen et al. (2013) and Roederer et al. (2014) as a guide, only one other star with such a low Ca abundance at [Fe/H] < -3.5 is known: HE 1424-0241, which has a similar metallicity but an even more extreme Ca underabundance of [Ca/Fe] = -0.50 (Cohen et al. 2007, 2013). The other 40 halo stars in this metallicity range are all at [Ca/Fe] ≥ 0.15 . HE 1424-0241 is not a perfect analog for the Sculptor stars because it is even more underabundant in Si than in Ca, at [Si/Fe] = -1.01, and has normal Mg and enhanced Mn and Co. Scl 11.1.4296, on the other hand, is deficient in Mg ([Mg/Fe] = -0.39) as well as the other α -elements, while Scl 07-50 has a low Si abundance but is not nearly as depleted as HE 1424-0241, and its Mn abundance is on the low end compared to typical halo stars (see above). Cohen et al. (2007) argue that HE 1424-0241 must have been enriched by a very small number of supernovae (SNe), with the Si-deficient material likely contributed by a supernova of around $35 M_{\odot}$.

The other known stars with α -element abundance patterns reminiscent of Scl 07-50 are the two stars in the ultra-faint dwarf galaxy Hercules studied by Koch et al. (2008). Those stars are substantially more metal-rich, at [Fe/H] ≈ -2 , but have high Mg and O abundances combined with low Ca, making for extreme [Mg/Ca] ratios. As with HE 1424-0241, Koch et al. (2008) suggest that this abundance pattern results from small numbers of SN explosions and a high-mass ($\sim 35 M_{\odot}$) progenitor.

4.3. Carbon

Neither of the two new Sculptor stars presented in this paper is carbon-rich (for Scl 6.6.402 we obtain only an upper limit on [C/Fe], but that is sufficient to rule out a substantial carbon enhancement). Starkenburg et al. (2013) recently analyzed a sample of seven Sculptor stars with $-3.5 < [\text{Fe}/\text{H}] < -2.5$, plus S1020549 and Scl 07-50, similarly finding no examples of stars with large carbon enhancements. They concluded that there is potential tension between the lack of identified carbon-enhanced metal-poor (CEMP) stars in Sculptor and the prevalence of such stars in the Milky Way, but a larger sample is needed for this result to be conclusive (also see Skúladóttir et al. 2014). Since we only add two additional non-carbon-enhanced EMP stars, the probability calculations they reported do not change significantly. A sample roughly twice as large will be necessary to deter-

⁶ The Ca triplet lines of Scl 07-50 are stronger than those of CD-38°245, but NLTE and 3D corrections for those lines are much larger and even less well understood.

⁷ The only outlier where Ca I 4226.73 Å and the other lines

have a significantly larger abundance difference is the coolest star, CS 22950-046, which is similar in temperature to Scl 07-50, raising the possibility of a sharp temperature dependence in the abundance derived from the resonance line. However, because the theoretical studies of Mashonkina et al. (2007), Merle et al. (2011), and Spite et al. (2012) do not indicate strong changes in NLTE corrections at $T_{\text{eff}} \sim 4500 \text{ K}$, we regard CS 22950-046 as a random outlier rather than a systematic one.

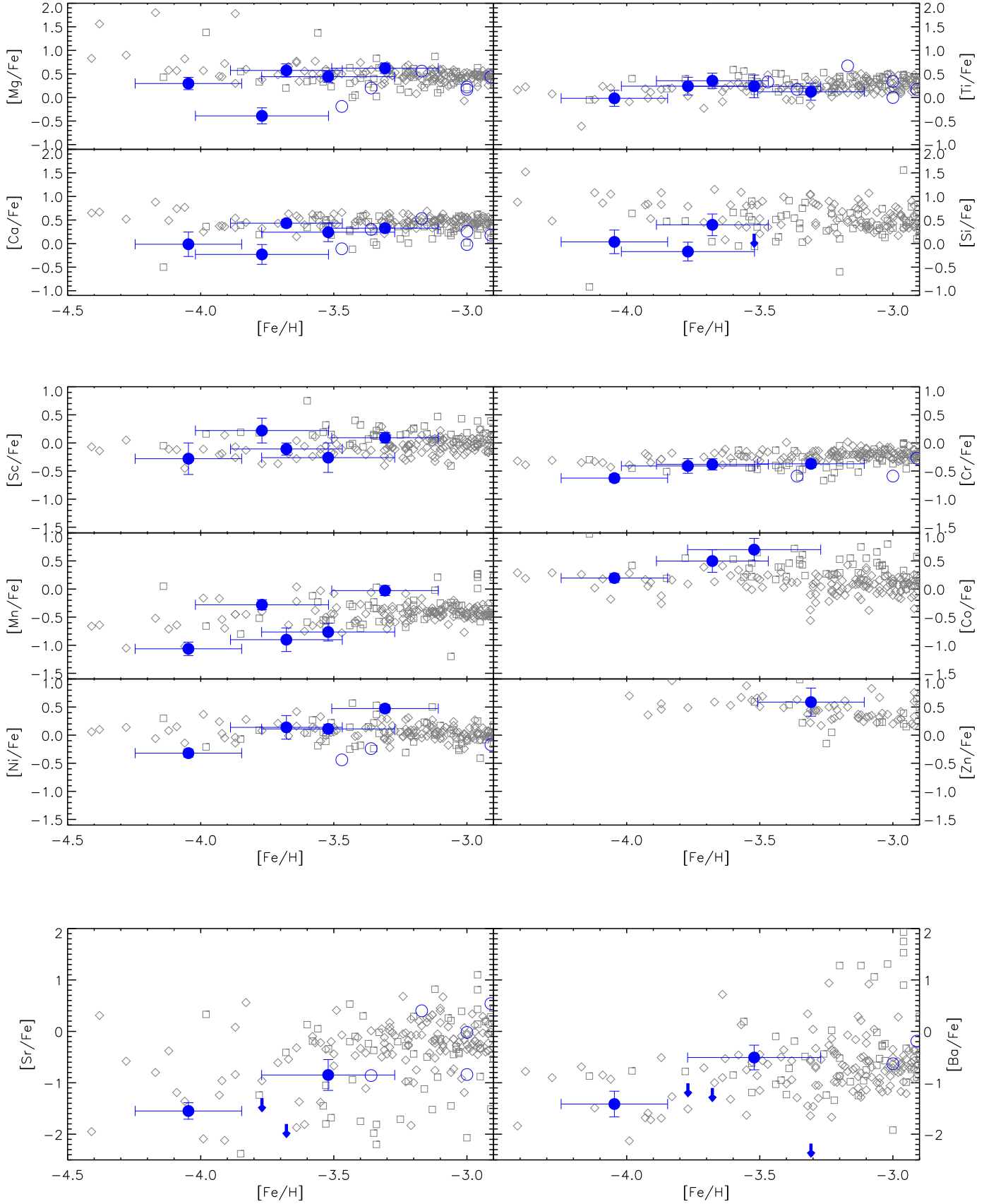


Figure 1. Abundance patterns of EMP stars in Sculptor (filled blue circles) compared to the Milky Way halo samples of Cohen et al. (2013, open gray squares) and Roederer et al. (2014, open gray diamonds). The Sculptor sample of Starkenburg et al. (2013) is plotted as open blue circles. The α -elements are displayed in the top set of panels, iron peak elements in the middle set of panels, and neutron-capture elements in the bottom panels. The Cohen et al. (2013) abundances have been adjusted to place them on the Asplund et al. (2009) solar abundance scale.

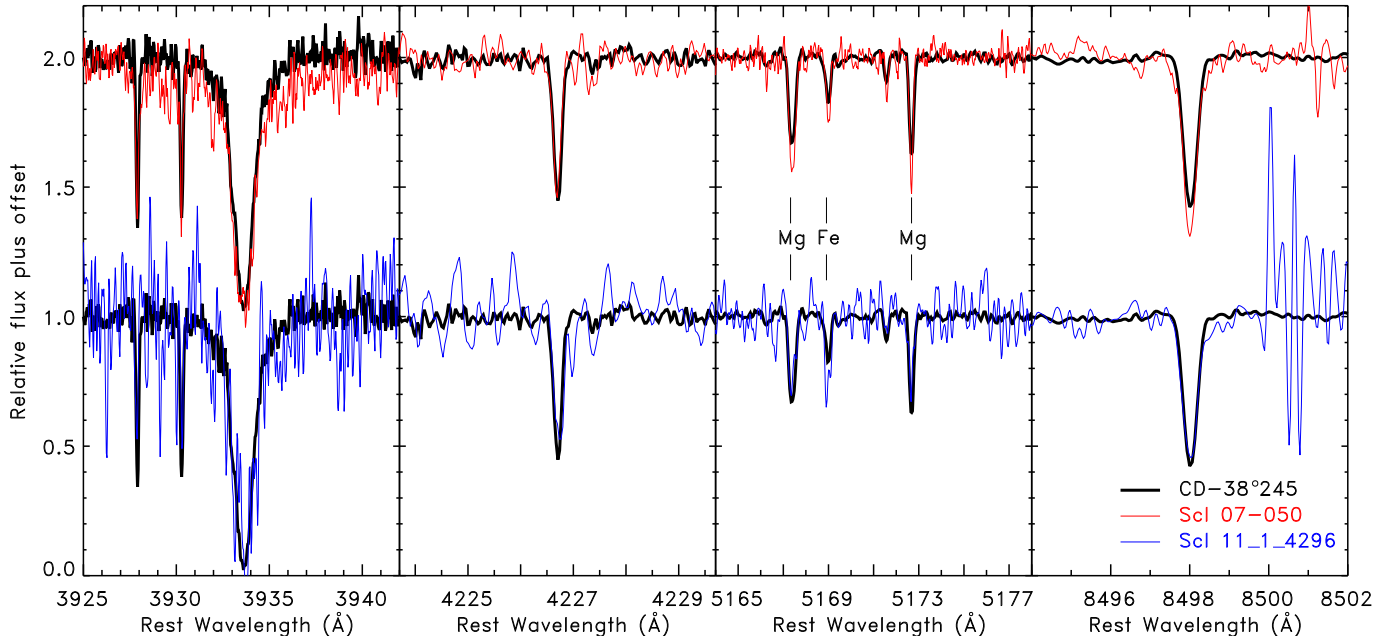


Figure 2. Spectra of the two most metal-poor stars in Sculptor, Scl 07-50 (red) and Scl 11_1_4296 (blue, smoothed slightly for cosmetic purposes), compared to CD-38°245. Ca K is plotted in the left panel, Ca I 4226.73 Å in the second panel, the bluer two lines of the Mg triplet in the third panel, and the bluest Ca II triplet line in the right panel.

mine whether the fraction of CEMP stars in Sculptor is truly discrepant with that of the halo.

4.4. Neutron-Capture Elements

Only a few neutron-capture species can be measured in our spectra. We detect the Sr II resonance lines in Scl 6_6_402 and Scl 07-50, with low abundances of $[\text{Sr}/\text{Fe}] = -0.85$ and $[\text{Sr}/\text{Fe}] = -1.55$ ($[\text{Sr}/\text{H}] = -4.37$ and $[\text{Sr}/\text{H}] = -5.60$), respectively. S1020549 has an even lower upper limit of $[\text{Sr}/\text{Fe}] < -1.66$ ($[\text{Sr}/\text{H}] < -5.48$). Ba is detected in the same two stars, with $[\text{Ba}/\text{Fe}]$ ratios and upper limits that are mostly closer to the halo averages than those for Sr. Eu upper limits rule out large enhancements of r-process elements but are not otherwise constraining.

These results generally fit in with the picture of very low abundances of neutron-capture elements in the most metal-poor stars in dwarf galaxies (Fulbright et al. 2004; Frebel et al. 2010a, 2014; Ishigaki et al. 2014). Sr in particular seems notably underabundant in our Sculptor sample.

4.5. Implications for the Early History of Sculptor

Considering our sample in conjunction with the seven additional Sculptor stars from Starkenburg et al. (2013), there is evidence for abundance spreads within the Sculptor EMP population in α -elements (Mg and Ca), iron peak elements (Ni), and neutron-capture elements (Sr and Ba). While comparisons to the Milky Way halo are hampered by the smaller sample size in Sculptor, and more importantly the lower data quality, Figure 1 suggests that the star-to-star scatter among Sculptor stars for a number of elements may be higher than in the halo. To investigate the significance of the increased scatter, we calculated the intrinsic scatter in $[\text{X}/\text{Fe}]$ for both EMP stars in the halo data sets of Cohen et al. (2013) and

Roederer et al. (2014) and the combined Sculptor sample from Starkenburg et al. (2013) and this paper. We used the method described by Kelly (2007) to determine the intrinsic scatter in a set of data points with non-uniform uncertainties in both variables. The elements for which halo EMP stars follow tight relations and there are more than five measurements available for Sculptor stars are Mg, Ca, Ti, Cr, and Ni.

For Mg, the handful of stars with highly enhanced abundances at $[\text{Fe}/\text{H}] < -3.5$ give the halo sample a significant intrinsic scatter of 0.17 dex. Still, the very low $[\text{Mg}/\text{Fe}]$ ratio of Scl 11_1_4296 and the low Mg abundances of several of the Starkenburg et al. (2013) stars result in a larger scatter for Sculptor of $\sigma = 0.36^{+0.14}_{-0.10}$ dex, which is significant at the 99% confidence level. The scatter of the halo stars in $[\text{Ca}/\text{Fe}]$ is slightly smaller (0.15 dex), but the outliers in Sculptor are less deviant, making the intrinsic scatter of the Sculptor stars larger at only 71% confidence. $[\text{Ti}/\text{Fe}]$ has even less scatter in the halo data (observed $\sigma_{[\text{Ti}/\text{Fe}]} = 0.14$ dex, intrinsic $\sigma_{[\text{Ti}/\text{Fe}]} = 0.10$ dex). The Sculptor stars generally follow the halo trend in $[\text{Ti}/\text{Fe}]$ closely, but the intrinsic scatter of $0.24^{+0.14}_{-0.11}$ dex is larger at 91% confidence. For Cr, we similarly find that the intrinsic scatter of the Sculptor stars of $\sigma = 0.18^{+0.16}_{-0.10}$ is larger than that of the halo ($\sigma = 0.10$ dex) at 80% confidence. Finally, for the iron-peak element Ni the larger uncertainties in $[\text{Ni}/\text{Fe}]$ leave very little room for any intrinsic scatter in the halo sample; we derive an intrinsic scatter of 0.04 ± 0.02 dex. The Sculptor stars, in contrast, have $\sigma = 0.46^{+0.35}_{-0.19}$, which is larger at 99.9% confidence. Given the still small sample of metal-poor stars in Sculptor, these differences are (with the exception of Mg and Ni) suggestive rather than definitive, and abundance patterns for more Sculptor stars will be needed to confirm their greater diversity

relative to the halo. Nevertheless, the apparently increased heterogeneity in the most metal-poor Sculptor stars highlights the likely role played by inhomogeneous mixing in the early Sculptor interstellar medium and the small number of SNe that contributed to its initial chemical enrichment.

The abundance patterns of the two most metal-poor stars also point to enrichment by a limited number of progenitor stars. The low Si, Ca, and Ni abundances of Scl 07-50 and the exceptionally low α abundances of Scl 11.1.4296 stand out strongly from the typical abundances of similar metallicity stars in the halo, which presumably represent the mean yield from a larger number of primordial SNe. To determine what kind of SNe could be responsible for this chemical makeup, we fit their abundances with the Population III SN models of Heger & Woosley (2010). The best fitting models for Scl 07-50 are all relatively high mass ($22.5 M_{\odot}$) stars, while Scl 11.1.4296 is better fit by a $\sim 10 M_{\odot}$ star. Models with lower mass progenitors for Scl 07-50 and higher mass progenitors for Scl 11.1.4296 have significantly higher χ^2 values. In both cases, the data are consistent with high energy hypernova explosions with $E \gtrsim 3 \times 10^{51}$ erg, although lower energy explosions are not excluded for Scl 11.1.4296. It is intriguing that significantly different progenitor properties are preferred for these two stars. Since the SNe from a normal stellar initial mass function (IMF) will be dominated by the lowest mass stars that can undergo core collapse ($\sim 8 - 10 M_{\odot}$), the larger mass for the star that enriched Scl 07-50 may suggest that the IMF in Sculptor at the earliest times was biased toward high masses. Geha et al. (2013) have shown that the ultra-faint dwarfs Hercules and Leo IV have a bottom-light IMF, which if extrapolated to the high mass regime would be top-heavy. No direct measurements for Sculptor have been made yet, but would clearly be of interest.

To quantify how many supernovae could have contributed to the enrichment of the α -poor EMP stars in Sculptor, we followed the method described by Koch et al. (2008). We randomly generated small populations of massive stars ($10 M_{\odot} \leq M \leq 100 M_{\odot}$) and used the Heger & Woosley (2010) metal-free supernova yields (with a randomly chosen explosion energy and mixing parameter for each star) to determine the mean abundance ratios that would result after these stars polluted a primordial gas cloud. For a Salpeter (1955) IMF, sub-solar [Ca/Fe] ratios like we observe for Scl 11.1.4296 are found in less than 1% of these simulations unless the number of supernovae is less than five. [Ca/Fe] < -0.2 is exceedingly rare even for a single supernova explosion. More top-heavy IMFs, which may be appropriate for dwarf galaxies (Wyse et al. 2002; Kalirai et al. 2013; Geha et al. 2013), modestly reduce the likelihood of producing extremely Ca-poor material. We conclude that Sculptor may have hosted only 1–4 SNe at the time that its most metal-poor known stars were formed.

5. SUMMARY AND CONCLUSIONS

We have determined chemical abundances for five of the most metal-poor stars in the Sculptor dSph, all at [Fe/H] < -3.2 . Two of these stars are new discoveries reported here for the first time, while three others are taken from the literature and re-analyzed. Our slightly

revised metallicity for one of the literature stars is below [Fe/H] = -4 , classifying it as the first ultra metal-poor star known in a galaxy other than the Milky Way.

The two lowest metallicity stars both have very unusual abundance patterns. The α elements Mg, Ca, and Si are all extremely depleted in Scl 11.1.4296, while Scl 07-50 has low Ca, Si, and Ni, but a more normal level of Mg. The unique abundance patterns of the most metal-poor stars suggests that [Fe/H] $\lesssim -3.7$ is the regime in which only a few SNe contributed to the enrichment of Sculptor, implying that the stars studied here are part of just the second generation the galaxy ever formed. These chemical signatures can be reproduced by enrichment from Population III SNe.

The Ca abundances of the two most metal-poor stars rely entirely on the Ca I resonance line at 4226Å, which is the only neutral Ca line detected in our spectra. Because the effects of NLTE on this line are uncertain, we compared the Ca II K, Ca I 4226, and Ca II triplet lines in the Sculptor stars with the ultra metal-poor giant CD-38°245, finding that the abundances we derive are qualitatively consistent with the relative line strengths. We then used a set of EMP halo stars with similar metallicity and temperature in which multiple Ca I lines are detected to show that the resonance line produces a Ca abundance that is on average 0.09 dex lower than the abundance determined from other lines. This value is consistent with the latest NLTE calculations.

Although the three more metal-rich stars individually appear quite similar to Milky Way halo stars in the same metallicity range, when taken together with other Sculptor EMP stars we show that the star-to-star scatter in the abundance of several elements is substantially higher than in the halo. We infer that the early chemical evolution of Sculptor was heavily influenced by inhomogeneous mixing and stochastic effects from small numbers of SNe.

This publication is based upon work supported by the National Science Foundation under grants AST-1108811 and AST-1255160. We thank the referee for suggestions that strengthened the paper. We thank Atish Kamble for contributing observations, Gary da Costa for the photometric catalog, and Andy McWilliam, Lyudmila Mashonkina, Juna Kollmeier, and Ian Roederer for helpful conversations. This research has made use of NASA's Astrophysics Data System Bibliographic Services.

Facilities: Magellan:II (MIKE)

REFERENCES

- Alonso, A., Arribas, S., & Martínez-Roger, C. 1999, A&AS, 140, 261
- Aoki, W., Arimoto, N., Sadakane, K., et al. 2009, A&A, 502, 569
- Asplund, M., Grevesse, N., Sauval, A. J., & Scott, P. 2009, ARA&A, 47, 481
- Barklem, P. S., Piskunov, N., & O'Mara, B. J. 2000, A&AS, 142, 467
- Beers, T. C., & Christlieb, N. 2005, ARA&A, 43, 531
- Bergemann, M., & Gehren, T. 2008, A&A, 492, 823
- Bernstein, R., Shtetman, S. A., Gunnels, S. M., Mochnacki, S., & Athey, A. E. 2003, Proc. SPIE, 4841, 1694
- Bessell, M. S., & Norris, J. 1984, ApJ, 285, 622
- Casey, A. R. 2014, Ph.D. Thesis, Australian National Univ.
- Castelli, F., & Kurucz, R. L. 2004, arXiv:astro-ph/0405087
- Cayrel, R., Depagne, E., Spite, M., et al. 2004, A&A, 416, 1117
- Cohen, J. G., Christlieb, N., Thompson, I., et al. 2013, ApJ, 778, 56

- Cohen, J. G., & Huang, W. 2009, *ApJ*, 701, 1053
Cohen, J. G., & Huang, W. 2010, *ApJ*, 719, 931
Cohen, J. G., McWilliam, A., Christlieb, N., et al. 2007, *ApJ*, 659, L161
Coleman, M. G., Da Costa, G. S., & Bland-Hawthorn, J. 2005, *AJ*, 130, 1065
Dekker, H., D'Odorico, S., Kaufer, A., Delabre, B., & Kotzlwski, H. 2000, *Proc. SPIE*, 4008, 534
Dressler, A., Bigelow, B., Hare, T., et al. 2011, *PASP*, 123, 288
Frebel, A., Casey, A. R., Jacobson, H. R., & Yu, Q. 2013, *ApJ*, 769, 57
Frebel, A., Christlieb, N., Norris, J. E., et al. 2006, *ApJ*, 652, 1585
Frebel, A., Kirby, E. N., & Simon, J. D. 2010a, *Nature*, 464, 72
Frebel, A., Simon, J. D., Geha, M., & Willman, B. 2010b, *ApJ*, 708, 560
Frebel, A., Simon, J. D., & Kirby, E. N. 2014, *ApJ*, 786, 74
Fulbright, J. P., Rich, R. M., & Castro, S. 2004, *ApJ*, 612, 447
Geha, M., Brown, T. M., Tumlinson, J., et al. 2013, *ApJ*, 771, 29
Gilmore, G., Norris, J. E., Monaco, L., et al. 2013, *ApJ*, 763, 61
Heger, A., & Woosley, S. E. 2010, *ApJ*, 724, 341
Helmi, A., Irwin, M. J., Tolstoy, E., et al. 2006, *ApJ*, 651, L121
Ishigaki, M. N., Aoki, W., Arimoto, N., & Okamoto, S. 2014, *A&A* in press (arXiv:1401.1265)
Kalirai, J. S., Anderson, J., Dotter, A., et al. 2013, *ApJ*, 763, 110
Kelly, B. C. 2007, *ApJ*, 665, 1489
Kelson, D. D. 2003, *PASP*, 115, 688
Kirby, E. N., & Cohen, J. G. 2012, *AJ*, 144, 168
Kirby, E. N., Guhathakurta, P., Bolte, M., Sneden, C., & Geha, M. C. 2009, *ApJ*, 705, 328
Kirby, E. N., Simon, J. D., Geha, M., Guhathakurta, P., & Frebel, A. 2008, *ApJ*, 685, L43
Koch, A., McWilliam, A., Grebel, E. K., Zucker, D. B., & Belokurov, V. 2008, *ApJ*, 688, L13
Lai, D. K., Bolte, M., Johnson, J. A., et al. 2008, *ApJ*, 681, 1524
Marshall, J. L., Burles, S., Thompson, I. B., et al. 2008, *Proc. SPIE*, 7014,
Mashonkina, L., Korn, A. J., & Przybilla, N. 2007, *A&A*, 461, 261
McWilliam, A., Preston, G. W., Sneden, C., & Searle, L. 1995, *AJ*, 109, 2757
Menzies, J. W., Feast, M. W., Whitelock, P. A., & Matsunaga, N. 2011, *MNRAS*, 414, 3492
Merle, T., Thévenin, F., Pichon, B., & Bigot, L. 2011, *MNRAS*, 418, 863
Norris, J. E., Gilmore, G., Wyse, R. F. G., Yong, D., & Frebel, A. 2010a, *ApJ*, 722, L104
Norris, J. E., Yong, D., Gilmore, G., & Wyse, R. F. G. 2010b, *ApJ*, 711, 350
Roederer, I. U., Frebel, A., Shetrone, M. D., et al. 2008, *ApJ*, 679, 1549
Roederer, I. U., Preston, G. W., Thompson, I. B., et al. 2014, *AJ*, 147, 136
Salpeter, E. E. 1955, *ApJ*, 121, 161
Simon, J. D., Frebel, A., McWilliam, A., Kirby, E. N., & Thompson, I. B. 2010, *ApJ*, 716, 446
Skúladóttir, Á., Tolstoy, E., Salvadori, S., et al. 2014, *A&A*, in press (arXiv:1411.7956)
Sneden, C. A. 1973, Ph.D. Thesis, Univ. Texas at Austin
Sobeck, J. S., Kraft, R. P., Sneden, C., et al. 2011, *AJ*, 141, 175
Spite, M., Andrievsky, S. M., Spite, F., et al. 2012, *A&A*, 541, A143
Starkenburger, E., Hill, V., Tolstoy, E., et al. 2010, *A&A*, 513, A34
Starkenburger, E., Hill, V., Tolstoy, E., et al. 2013, *A&A*, 549, A88
Tafelmeyer, M., Jablonka, P., Hill, V., et al. 2010, *A&A*, 524, A58 (T10)
Tolstoy, E., Irwin, M. J., Helmi, A., et al. 2004, *ApJ*, 617, L119
Unsöld, A. 1955, Berlin, Springer, 1955. 2. Aufl.
Wyse, R. F. G., Gilmore, G., Houdashelt, M. L., et al. 2002, *NewA*, 7, 395
Yong, D., Norris, J. E., Bessell, M. S., et al. 2013, *ApJ*, 762, 26

Table 2
Equivalent Widths (abridged)

Species	λ [Å]	χ [eV]	$\log gf$ [dex]	EW (mÅ)	$\log \epsilon$ (dex)	EW (mÅ)	$\log \epsilon$ (dex)	EW (mÅ)	$\log \epsilon$ (dex)	EW (mÅ)	$\log \epsilon$ (dex)	EW (mÅ)	$\log \epsilon$ (dex)
				Scl 11.1.4296	Scl 6.6.402	Scl 07-50	Scl 07-49	S1020549					
CH	4313.00	syn	5.00	syn	<5.50	syn	4.10	syn	<4.95
CH	4325.00	syn	<5.50	syn	<4.47	syn	<5.25
Na I	5889.95	0.00	0.11	79.3	2.40	97.5	2.90	82.3	2.19	123.3	2.72	102.4	2.68
Na I	5895.92	0.00	-0.19	65.3	2.45	71.2	2.69	59.1	2.12	106.6	2.73	83.1	2.64
Mg I	3829.36	2.71	-0.21	83.4	3.61	98.7	3.80
Mg I	3832.30	2.71	0.27	97.0	3.46
Mg I	3838.29	2.72	0.49	131.9	3.86
Mg I	5172.68	2.71	-0.45	65.9	3.32	119.9	4.43	107.4	3.87	185.4	4.95	129.3	4.39
Mg I	5183.60	2.72	-0.24	78.7	3.36	145.5	4.61	117.6	3.87	196.0	4.87	154.3	4.60
Mg I	5528.40	4.34	-0.50	55.8	4.92
Al I	3944.01	0.00	-0.62	syn	2.02	syn	1.32	syn	<2.00
Al I	3961.52	0.01	-0.34	59.4	1.68	syn	<2.42	syn	1.40	syn	<1.90
Si I	3905.52	1.91	-1.09	87.2	3.57	syn	<4.20	syn	3.50	syn	4.23
Si I	4102.94	1.91	-3.14	syn	<5.08	syn	<3.92	syn	<4.50
Ca I	4226.73	0.00	0.24	97.5	2.25	126.4	2.97	108.6	2.19	149.2	3.11
Ca I	4434.96	1.89	-0.01	57.3	<4.32	32.4	3.15
Ca I	5588.76	2.52	0.21	24.8	3.35
Ca I	5594.47	2.52	0.10	13.1	3.23
Ca I	6102.72	1.88	-0.79	19.1	3.40
Ca I	6122.22	1.89	-0.32	37.4	3.32	16.0	2.99
Ca I	6162.17	1.90	-0.09	57.3	3.42
Ca I	6439.07	2.52	0.47	37.2	3.30	17.7	2.99
Sc II	4246.82	0.32	0.24	81.6	-0.40	syn	-0.80	syn	-1.13	syn	-0.73
Sc II	4314.08	0.62	-0.10	syn	-0.55	syn	-1.20	syn	-0.63
Sc II	4325.00	0.59	-0.44	syn	-0.55	syn	-1.20	syn	-0.73
Sc II	4400.39	0.61	-0.54	syn	-0.78
Sc II	4415.54	0.59	-0.67	syn	<-0.74	syn	-0.31
Sc II	5031.01	1.36	-0.40	syn	<-0.44	syn	-0.18
Sc II	5526.79	1.77	0.02	syn	0.05
Sc II	5657.91	1.51	-0.60	syn	<0.11

Note. — Only a portion of the table is shown in the arXiv version of the paper. Please contact the first author or refer to the published version for the full table.

Table 3
Abundances

Species	Scl 11.1_4296				Scl 6.6_402				Scl 07-50				Scl 07-49				S1020549			
	[X/Fe] [dex]	log $\epsilon(X)$ [dex]	No. lines	σ^a [dex]	[X/Fe] [dex]	log $\epsilon(X)$ [dex]	No. lines	σ^a [dex]	[X/Fe] [dex]	log $\epsilon(X)$ [dex]	No. lines	σ^a [dex]	[X/Fe] [dex]	log $\epsilon(X)$ [dex]	No. lines	σ^a [dex]	[X/Fe] [dex]	log $\epsilon(X)$ [dex]	No. lines	σ^a [dex]
C(CH)	0.34	5.00	1	...	< 0.59	< 5.50	1	...	-0.28	4.10	1	< 0.20	< 4.95	1	...
Na I	-0.04	2.43	2	0.03	0.08	2.80	2	0.15	-0.03	2.16	2	0.05	-0.20	2.73	2	0.01	0.10	2.66	2	0.03
Mg I	-0.39	3.44	4	0.11	0.44	4.52	2	0.13	0.30	3.85	4	0.03	0.62	4.91	3	0.04	0.58	4.50	2	0.15
Al I	-1.00	1.68	1	...	-0.91	2.02	1	...	-1.04	1.36	2	0.06	< -0.87	< 1.90	1	...
Si I	-0.17	3.57	1	...	< 0.21	< 4.20	1	...	0.04	3.50	1	0.40	4.23	1	...
Ca I ^b	-0.23	2.34	1	...	0.24	3.06	1	...	-0.01	2.28	1	...	0.33	3.36	5	0.05	0.43	3.09	5	0.10
Sc II	0.22	-0.40	1	...	-0.26	-0.63	3	0.14	-0.28	-1.18	3	0.04	0.09	-0.07	2	0.16	-0.11	-0.64	5	0.19
Ti I	0.06	1.70	5	0.09	0.48	1.75	2	0.01
Ti II	0.23	1.41	11	0.12	0.24	1.67	4	0.23	-0.01	0.89	10	0.11	0.19	1.83	6	0.10	0.34	1.61	18	0.22
Cr I	-0.41	1.46	3	0.19	-0.62	0.97	4	0.12	-0.37	1.96	2	0.06	-0.38	1.58	5	0.20
Mn I ^c	-0.28	1.38	2	0.10	-0.77	1.14	3	0.23	-1.06	0.32	3	0.16	-0.02	2.10	2	0.11	-0.90	0.85	1	...
Fe I ^d	-3.77	3.73	54	0.32	-3.52	3.98	44	0.24	-4.05	3.45	54	0.10	-3.31	4.19	92	0.14	-3.68	3.82	84	0.24
Fe II ^d	-3.76	3.74	2	0.10	-3.52	3.98	4	0.09	-4.04	3.46	4	0.13	-3.28	4.22	5	0.11	-3.67	3.83	5	0.16
Co I	0.70	2.17	1	...	0.20	1.14	3	0.08	0.50	1.81	1	...
Ni I	0.11	2.81	2	0.10	-0.32	1.85	3	0.11	0.48	3.39	4	0.14	0.14	2.68	1	...
Zn I	0.59	1.84	1
Sr II	< -1.30	< -2.20	1	...	-0.85	-1.50	1	...	-1.55	-2.73	2	0.04	< -1.80	< -2.61	1	...
Ba II	< -1.01	< -2.60	1	...	-0.51	-1.85	1	...	-1.41	-3.28	1	...	< -2.18	< -3.31	1	...	< -1.10	< -2.60	1	...
Eu II	< 1.29	< -1.71	1	...	< 0.76	< -2.77	1	< 1.00	< -2.16	1	...

^a Dispersion of the abundance ratio about the mean for species where multiple lines were detected.

^b An NLTE correction of +0.09 dex was applied to Ca I abundances determined only from the 4226.73 Å line (see § 4.2).

^c An NLTE correction of +0.3 dex was applied to abundances determined from the 4030 Å triplet lines.

^d Abundances are relative to hydrogen for Fe I and Fe II.